

Synergetic Effect of Host–Guest Chemistry and Spin Crossover in 3D Hofmann-like Metal–Organic Frameworks [Fe(bpac)M(CN)₄] (M = Pt, Pd, Ni)**

Carlos Bartual-Murgui,^[a, b] Lionel Salmon,^[a] Amal Akou,^[a] Norma A. Ortega-Villar,^[b, c] Helena J. Shepherd,^[a] M. Carmen Muñoz,^[d] Gábor Molnár,^[a] José Antonio Real,^{*, [b]} and Azzedine Bousseksou^{*, [a]}

Abstract: The synthesis and characterization of a series of three-dimensional (3D) Hofmann-like clathrate porous metal–organic framework (MOF) materials [Fe(bpac)M(CN)₄] (M = Pt, Pd, and Ni; bpac = bis(4-pyridyl)acetylene) that exhibit spin-crossover behavior is reported. The rigid bpac ligand is longer than the previously used azopyridine and pyrazine and has been selected with the aim to improve both the spin-crossover properties and the porosity of the corresponding porous coordination polymers (PCPs). The 3D network is composed of successive {Fe[M(CN)₄]}_n planar layers bridged by the bis-monodentate bpac ligand linked in the apical positions of the iron center. The large void between the layers, which represents 41.7% of the unit cell, can accommodate solvent

molecules or free bpac ligand. Different synthetic strategies were used to obtain a range of spin-crossover behaviors with hysteresis loops around room temperature; the samples were characterized by magnetic susceptibility, calorimetric, Mössbauer, and Raman measurements. The complete physical study reveals a clear relationship between the quantity of included bpac molecules and the completeness of the spin transition, thereby underlining the key role of the π – π stacking interactions operating between the host and guest bpac molecules within the network. Al-

though the inclusion of the bpac molecules tends to increase the amount of active iron centers, no variation of the transition temperature was measured. We have also investigated the ability of the network to accommodate the inclusion of molecules other than water and bpac and studied the synergy between the host–guest interaction and the spin-crossover behavior. In fact, the clathration of various aromatic molecules revealed specific modifications of the transition temperature. Finally, the transition temperature and the completeness of the transition are related to the nature of the metal associated with the iron center (Ni, Pt, or Pd) and also to the nature and the amount of guest molecules in the lattice.

Keywords: adsorption • host–guest systems • metal–organic frameworks • microporous materials • spin crossover

Introduction

Increasing attention is being paid to three-dimensional porous coordination polymers (PCPs), also called metal–organic frameworks (MOFs),^[1] in particular for materials exhibiting spin-crossover (SCO) properties.^[2] Among them, Hofmann-like SCO-PCPs are unique in several respects:

1) they show complete cooperative thermal bistability at room temperature with large hysteresis loops up to approximately 50 K;^[3] 2) the spin state can be switched by irradiating the sample with a pulsed laser within the hysteresis loop;^[4] 3) a reversible switching between the high-spin and low-spin states at the Fe^{II} sites takes place concomitantly with the uptake of guest molecules;^[5] 4) these materials can

[a] Dr. C. Bartual-Murgui, Dr. L. Salmon, A. Akou, Dr. H. J. Shepherd, Dr. G. Molnár, Dr. A. Bousseksou
Laboratoire de Chimie de Coordination
CNRS UPR-8241 and Université de Toulouse
UPS, INPT, 31077 Toulouse (France)
E-mail: azzedine.bousseksou@lcc-toulouse.fr

[b] Dr. C. Bartual-Murgui, Dr. N. A. Ortega-Villar, Prof. Dr. J. A. Real
Instituto de Ciencia Molecular (ICMol)
Universidad de Valencia
C/Catedrático José Beltrán Martínez 2
46980 Paterna (Valencia) (Spain)
E-mail: jose.a.real@uv.es

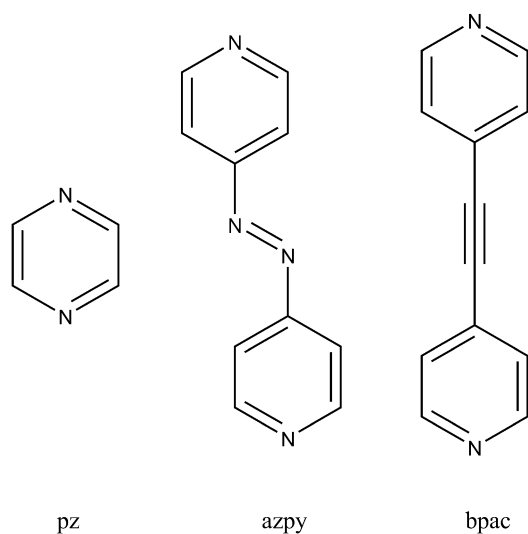
[c] Dr. N. A. Ortega-Villar
Departamento de Química Inorgánica
Universidad Autónoma de México (UNAM)
México D. F., 04510 (México)

[d] Prof. Dr. M. C. Muñoz
Departamento de Física Aplicada
Universitat Politècnica de València
Camino de Vera s/n, 46022, Valencia (Spain)

[**] bpac = bis(4-pyridyl)acetylene.

 Supporting information for this article is available on the WWW under <http://dx.doi.org/10.1002/chem.201102357>. It contains additional crystallographic data and crystal structure views, thermogravimetric analyses, and Raman spectra.

be prepared as nanocrystals,^[6] nanoparticles,^[7] and continuous or nano-patterned thin films,^[8] while still retaining the SCO properties. The versatility of the properties of such Hofmann-like SCO-PCPs has been demonstrated in the series $\{\text{Fe}(\text{azpy})[\text{M}(\text{CN})_4]\cdot n\text{H}_2\text{O}$ ($\text{M}=\text{Ni}, \text{Pd}, \text{Pt}$; $\text{azpy}=4,4'$ -azopyridine),^[9] which displays enhanced porosity but remarkably lower cooperativity than the pyrazine (pz) series $\{\text{Fe}(\text{pz})[\text{M}(\text{CN})_4]\cdot n\text{H}_2\text{O}$,^[2a] this is likely a result of the flexible nature of the azpy ligand. Belonging to this family of compounds, the pillared ligand of the title compounds has been chosen to affect both the SCO properties and the capacity to sense invited molecules. Indeed, the bis(4-pyridyl)acetylene (bpac) ligand is rigid and longer than azpy and



pz and so it should improve both the cooperativity and the porosity of the corresponding PCP materials. In recent reports, we have described the structural and magnetic properties of the novel $\{\text{Fe}(\text{bpac})[\text{Pt}(\text{CN})_4]\}$ ^[3a] and $\{\text{Fe}(\text{bpac})_2[\text{Ag}(\text{CN})_2]\}$ ^[10] compounds. Similarly to the previously reported 3D porous SCO coordination Hofmann polymers $\{\text{Fe}(\text{L})[\text{Pt}(\text{CN})_4]\}$ ($\text{L}=\text{pz}$,^[4b] azpy ^[9]), the crystal of the Pt/bpac derivative belongs to the tetragonal $P4/mmm$ space group. The structure is comprised of an almost regular octahedral $[\text{Fe}^{\text{II}}\text{N}_6]$ site and a square-planar site defined by the anion $[\text{Pt}(\text{CN})_4]^{2-}$ (Figure 1). The equatorial positions of the octahedron are occupied by four nitrogen atoms of four equivalent $[\text{Pt}(\text{CN})_4]^{2-}$ groups, which act as bridges linking four iron(II) atoms that generate $\{\text{Fe}[\text{Pt}(\text{CN})_4]\}_\infty$ layers. The layers lie on top of each other and are pillared by the ligand bpac, which occupies the axial positions of the iron(II), thus generating the porous 3D framework. The accessible volume without invited molecules (293.6 \AA^3) corresponds to 41.7% of the unit cell at 120 K, which is more than twice the accessible volume of the homologous pz derivative.^[4] This volume is partially occupied by molecules of bpac localized in the channels with their aromatic rings in front of those of the pillared bpac ligands, so that π - π stacking inter-

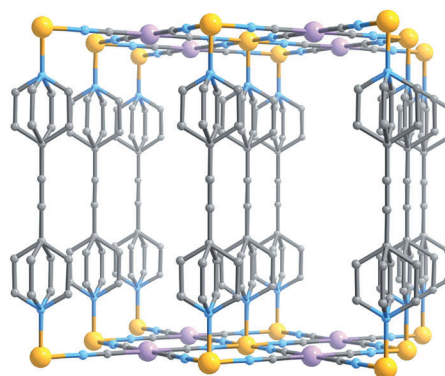


Figure 1. Perspective of a fragment of $\{\text{Fe}(\text{bpac})[\text{Pt}(\text{CN})_4]\}$ coordination polymer. The inclusion of bpac has been omitted for clarity (color code: Fe, yellow; Pt, lilac; N, blue; C, gray).

action is observed. In the present paper, we show a complete study of this new series of SCO Hofmann-like coordination polymers $\{\text{Fe}(\text{bpac})[\text{M}(\text{CN})_4]\}$ ($\text{M}=\text{Pt}, \text{Pd}, \text{and Ni}$). We present different synthetic methods, the study of the composition, as well as the structural and physical characterization of the compounds. It is shown how small variations of the synthetic procedure may give rise to materials that differ considerably in composition and physical behavior. Moreover, with the aim of studying the synergetic effect of the host-guest chemistry and the spin-crossover phenomenon, different strategies have been developed for the inclusion of various guest molecules in these three-dimensional networks.

Results and Discussion

Synthesis and characterization: Although several methods for the synthesis of the bpac ligand are found in the literature,^[11] we have developed a new method^[3] inspired by the palladium-catalyzed coupling reaction of haloheteroaromatic ligands reported by N. Inoue et al.^[12] The advantages of this three-step method (see Scheme S1 in the Supporting Information) are the possibility of working with water as a solvent and the excellent yields of the coupling reaction. The bpac ligand was prepared in 38% total yield for the three steps.

Thereafter, two different synthetic approaches have been used to obtain complexes with different composition. According to the first synthetic method (method A), treatment of a solution of iron(II) tetrafluoroborate salt containing the bpac ligand with a solution containing the $\text{K}_2[\text{M}(\text{CN})_4]$ ($\text{M}=\text{Ni}, \text{Pd}, \text{or Pt}$) salt at a controlled addition speed of 1 mL per minute afforded the corresponding $\{\text{Fe}(\text{bpac})[\text{M}(\text{CN})_4]\cdot \text{H}_2\text{O}\cdot x(\text{bpac})$ ($\text{M}=\text{Pt}, x=0.71$ (**1**); $\text{M}=\text{Pd}, x=0.78$ (**2**); $\text{M}=\text{Ni}, x=0.40$ (**3**)) compounds, in which x was determined by elemental analyses. The deviation of the Pt/Fe ratio up to 0.97 and the concomitant detection of traces of boron atoms by elemental analyses are in agreement with the presence of $[\text{Pt}(\text{CN})_4]^{2-}$ vacancies and the related pres-

ence of BF_4^- anions according to charge neutrality. This hypothesis also corroborates the low nitrogen percentage found for most of the samples. The quantity of included water molecules was measured by thermogravimetric analyses (see Figure S1 in the Supporting Information) and approximately one molecule per iron(II) ion was found for all compounds. Moreover, above 500 K, a significant loss of mass can be attributed to a fraction of included bpac molecules. One should note that the syntheses have been reproduced many times and the obtained products appeared to have slightly different stoichiometry. Nevertheless, general tendencies can be established as a function of the synthetic method used (see magnetic measurements, discussed below). As confirmed by the large quantity of included bpac molecules (x) in samples **1–3**, syntheses following method A were carried out with a continuous excess amount of bpac during the addition of the metalocyanate salt. With the aim of limiting this inclusion, an alternative method B was used, which consisted of adding a solution containing both iron(II) tetrafluoroborate salt and bpac ligand to a solution of $\text{K}_2[\text{Pt}(\text{CN})_4]$ salt. In this case, as expected, a quite different composition $\{\text{Fe}(\text{bpac})[\text{Pt}(\text{CN})_4]\cdot\text{H}_2\text{O}\cdot 0.09(\text{bpac})$ (**4**) with a significantly lower quantity of included bpac molecules was obtained. Although the quantity of included bpac molecules differs depending on whether method A or B was used, no significant effect was observed on the quantity of vacancies of $[\text{Pt}(\text{CN})_4]^{2-}$. In the following studies of the physical properties and experiments of guest inclusion, compounds **1'** and **1''** (**4'** and **4''**) correspond to samples formed in the same manner as sample **1** (**4**), but with slightly different compositions. As an example, Figure 2 shows the color change of sample **1** from red to yellow when passing from the low-spin (LS) to the high-spin (HS) state.



Figure 2. Photographs of powder samples of **1** in both spin states.

X-ray powder diffraction: Powder X-ray diffraction patterns of samples **1–3** at 298 K are shown in Figure 3. Their similarities demonstrate the close structural relationship of the Pt, Pd, and Ni derivatives, also confirmed by Raman spectroscopy. Subtle differences for the nickel derivative may be explained by the more important distortion of the network in agreement with the lower ionic radius than the platinate and palladate derivatives. The X-ray powder diffraction profile of **1** was satisfactorily fitted in the temperature range of 150 to 400 K using the tetragonal $P4/mmm$ model ($a=b=7.42(1)$, $c=14.06(1)$ Å; $V=774.5(7)$ Å³ at 380 K) in agreement with the result of the single-crystal X-ray measurement.^[3a] During the HS-to-LS transition, the unit-cell parameters show a decrease of 3.3 and 2.6% measured for

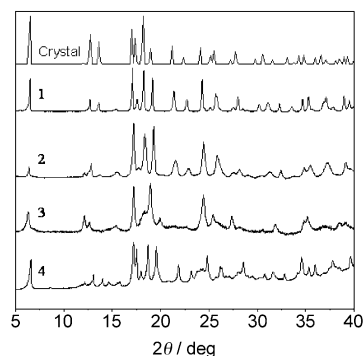


Figure 3. X-ray powder diffraction patterns of **1–4** measured at 298 K and calculated from single-crystal data at 120 K.

$a(b)$ and c axes, respectively. However, no thermal expansion was measured between 148 and 223 K in the low-spin state and very small thermal expansion was measured between 340 and 400 K in the high-spin state. This unusual phenomenon was also reported in the pyrazine derivative $[\text{Fe}(\text{pz})\text{Pt}(\text{CN})_4]$,^[4b] and has been explained in other compounds containing a cyanide-bridged framework as stemming from the great flexibility of the cyanide bridge.^[13] Figure S2 in the Supporting Information shows the thermal variation of the volume of the unit cell for compound **1**, which increases significantly during the spin transition (69 Å³, 9.7%). This value is large compared to the generally observed 1–6% variation in SCO complexes with FeN_6 coordination polyhedra,^[14] although similar in magnitude to the pyrazine and azopyridine derivatives (13 and 9.3%, respectively). The largest increase in the case of the pyrazine derivative can be explained by the rather small unit-cell volume of the complex. This increase of the unit-cell volume is essentially ascribed to the increase of Fe–N bond lengths (0.2 Å on average) upon spin transition since thermal expansion is relatively insignificant in the investigated temperature range. Figure 3 also shows powder X-ray diffraction patterns of **4** (method B) at 298 K. Although all the patterns are clearly related, most notably with the characteristic peak at $2\theta=6.50^\circ$ indexed as the (001) reflection, there are also differences in the peak widths between the patterns that may be attributed to greater disorder within the sample with an increasing proportion of defects.

Differential scanning calorimetry (DSC) analysis: The calorimetric data (Figure 4) were recorded in the heating and cooling modes at 5 K min^{-1} to evaluate the enthalpy (ΔH) and entropy (ΔS) variations associated with the spin transitions of **1–3** in the hydrated and dehydrated forms (which were obtained by heating at 400 K). For **3**, the DSC curve shows a singularity at $T_c=275$ K both for the cooling and heating modes. It was not possible to observe any singularity for the dehydrated form of sample **3** due to the gradual nature of the spin crossover (see magnetic measurements below). The platinum and palladium derivative samples in the hydrated form show several maxima in the heating and cooling modes ($T_{c1}\uparrow=312$ K, $T_{c2}\uparrow=323$ K and $T_{c1}\downarrow=306$ K,

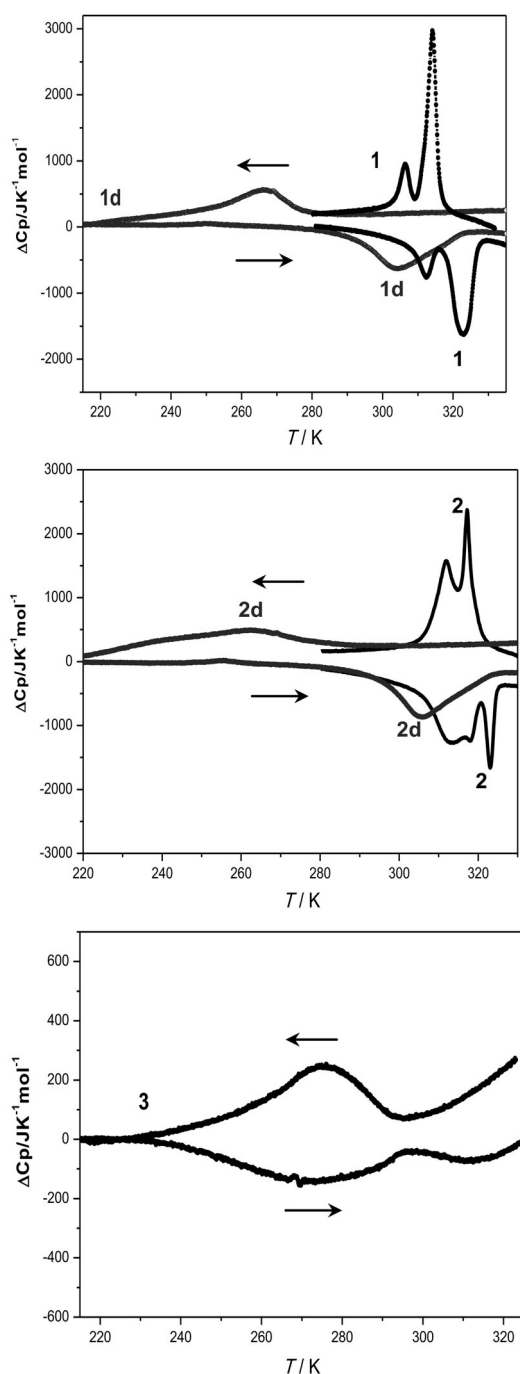


Figure 4. Calorimetric analysis for $\{\text{Fe}(\text{bpac})[\text{M}(\text{CN})_4]\}_n\text{H}_2\text{O}$ ($\text{M}=\text{Pt}$, Pd , or Ni) powders upon heating and cooling. Pt: **1** ($n=1$), **1d** ($n=0$); Pd: **2** ($n=1$), **2d** ($n=0$); Ni: **3** ($n=1$).

$T_{c2\downarrow}=314\text{ K}$ for **1**; $T_{c1\uparrow}=313\text{ K}$, $T_{c2\uparrow}=317\text{ K}$, $T_{c3\uparrow}=323\text{ K}$ and $T_{c1\downarrow}=311\text{ K}$, $T_{c2\downarrow}=317\text{ K}$ for **2**. For the dehydrated forms (**1d**, **2d**) only one maximum in both heating and cooling modes was observed ($T_{c\uparrow}=305\text{ K}$, and $T_{c\downarrow}=266\text{ K}$ for **1d**; $T_{c\uparrow}=308\text{ K}$ and $T_{c\downarrow}=261\text{ K}$ for **2d**). In comparison with the magnetic measurements, the slight deviation of the transition temperature could be associated with the difference of the heating and cooling rates. The multistep features observed in the calorimetric measurements might be an in-

dication of subtle structural modifications taking place concomitantly with the spin crossover and related to the presence of water molecules. The estimated ΔH and ΔS variations measured in the hydrated forms are 11 and 35; 13 and 41; and 4 kJ mol^{-1} and 16 $\text{J K}^{-1}\text{mol}^{-1}$ for **1**, **2**, and **3**, respectively. These values are common for iron(II) spin-crossover compounds; the small values observed for the nickel derivative are in agreement with a more incomplete spin transition.

Raman spectroscopy: Raman spectra of the dehydrated compounds (**1d–3d**), recorded between 200 and 2250 cm^{-1} , display similar features as shown in Figure S3 in the Supporting Information (see also Table S1 in the Supporting Information). In general, the Raman spectra of the bpac, pz, and azpy derivatives are quite similar below 600 cm^{-1} for a given metal M ($\text{M}=\text{Ni}$, Pd , or Pt) because these modes are associated mainly with metal–ligand vibration. In particular, Raman modes of **1d** (**2d**) around 495 (474) and 405 (395) cm^{-1} in the LS state are assigned to metal–ligand vibrations with the main involvement coming from δ_{MCN} bending and $\nu_{\text{Fe–NC}}$ stretching modes, respectively. In the HS state these modes shift to 342 (322) and 218 (214) cm^{-1} , which is in good agreement with the observations made earlier on the respective pyrazine homologues.^[3b] Between 600 and 1700 cm^{-1} , vibrational modes are attributed to the bpac ring stretching, bending, or twisting, through taking into account the spectrum of the pure bpac ligand and the Raman study of the azopyridine and pyrazine derivatives.^[9] In this region, and especially for Raman modes of the internal bpac ligand between 950 and 1700 cm^{-1} , clear variations of intensities are observed when going from the LS to the HS state. In particular, the HS mode at 1014 cm^{-1} (assigned to ring breathing), exhibits in the LS state a frequency shift to 1028 cm^{-1} . In Figure 5, the Raman spectrum of compounds **1d** (method A) and **4d** (method B) in the $950\text{–}1040\text{ cm}^{-1}$ region at 313 K are compared (with that of the pure ligand bpac). The vibrational mode at 992 cm^{-1} in compound **1d** is consistent with the vibrational mode of the guest bpac ligand, whereas the mode at 1014 cm^{-1} is attributed to the coordinated bpac ligand. Conversely, two modes at 1008 and

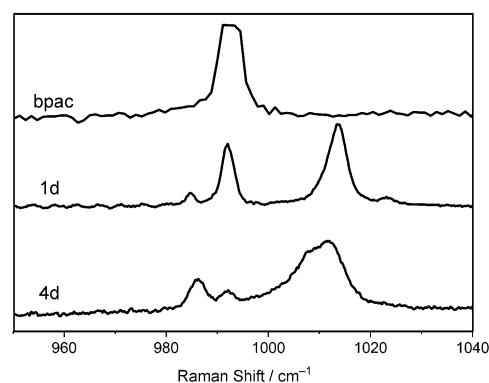


Figure 5. Selected region of the Raman spectrum of **1d** and **4d** at room temperature (with the spectrum of the bpac ligand for comparison).

1014 cm^{-1} can be ascribed to the breathing of the coordinated bpac ligand in **4d**, which is in agreement with the occurrence of a dissymmetric ligand coordination previously suggested. Moreover, the weak intensity of the mode at 992 cm^{-1} confirms the small fraction of included bpac molecules in **4d**. The temperature dependence of the normalized Raman intensity ratio $I_{1014 \text{ cm}^{-1}}/(I_{1014 \text{ cm}^{-1}} + I_{1028 \text{ cm}^{-1}})$ reported in Figure S4 in the Supporting Information for **1d** and **4d** and showing $T_{c\downarrow} = 242 \text{ K}$ and $T_{c\uparrow} = 308 \text{ K}$ and $T_{c\downarrow} = 235$ and $T_{1/2\uparrow} = 260 \text{ K}$, respectively, corroborates the magnetic and calorimetric data.

Magnetic measurements: $\chi_M T$ versus T plots (χ_M is the molar magnetic susceptibility) for **1–3** are displayed in Figure 6. The magnetic measurements were performed by

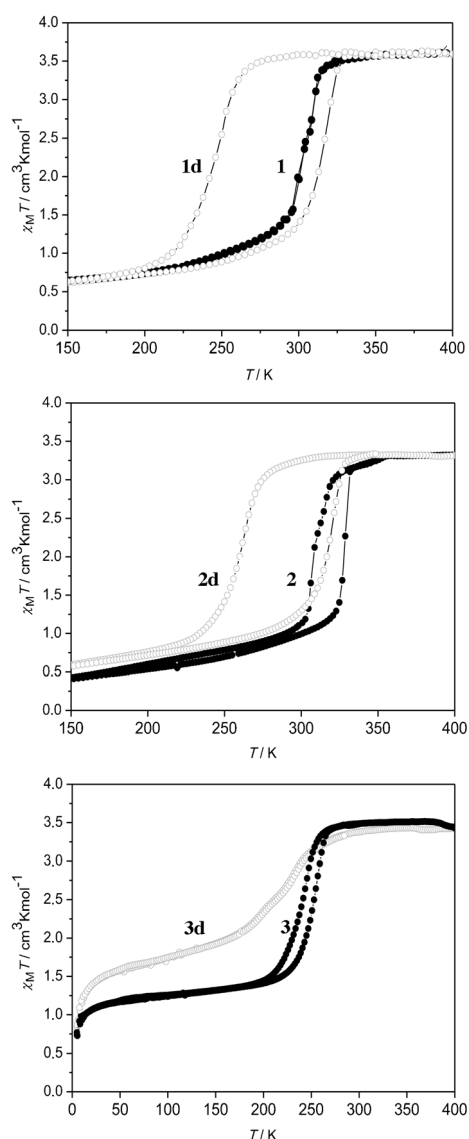


Figure 6. Magnetic properties, in the form of $\chi_M T$ versus T curves, of $[\text{Fe}(\text{bpac})[\text{M}(\text{CN})_4]] \cdot n\text{H}_2\text{O}$ ($\text{M} = \text{Pt}, \text{Pd}, \text{or Ni}$) powders upon heating and cooling. Pt: **1** ($n=1$), **1d** ($n=0$); Pd: **2** ($n=1$), **2d** ($n=0$); Ni: **3** ($n=1$), **3d** ($n=0$).

first cooling the sample from 340 K until 5 K and then heating from 5 K to 400 K at 2 K min^{-1} . At 340 K, for each sample, the $\chi_M T$ value is typical of iron(II) HS compounds ($3.20\text{--}3.50 \text{ cm}^3 \text{ K mol}^{-1}$), whereas at 50 K it is typical for an iron(II) ion in the LS state with a possible small residual fraction of iron(II) centers in the HS state: 0.50, 0.45, and $1 \text{ cm}^3 \text{ K mol}^{-1}$ for **1**, **2** and **3**, respectively. The transition temperature is $T_c = 303 \text{ K}$ for **1**, whereas a hysteresis is observed for **2** (20 K) and **3** (13 K): $T_{c\downarrow} = 308$ (**2**) and 238 K (**3**) and $T_{c\uparrow} = 328 \text{ K}$ (**2**), and 251 K (**3**) for the cooling and heating modes, respectively. According to the thermogravimetric data, a water molecule is lost at approximately 390 K in each compound. To investigate the role of this molecule in the SCO, the samples were kept at 400 K in the superconducting quantum interference device (SQUID) magnetometer for 60 min to dehydrate them in situ. Then, a subsequent cooling–heating cycle was performed to determine the magnetic behavior of the dehydrated samples **1d–3d** (Figure 6). The dehydrated forms **1d** and **2d** show spin crossover with a large hysteresis of 68 and 57 K, respectively. The transition temperatures are $T_{c\downarrow} = 246$ (**1d**) and 260 K (**2d**), and $T_{c\uparrow} = 314$ (**1d**) and 317 K (**2d**), whereas the barycenters of the hysteresis loops ($T_c = (T_{c\downarrow} + T_{c\uparrow})/2$), experience a relatively small decrease ($T_c = 280$ (**1d**) and 289 K (**2d**)), still remaining near room temperature. This contrasts with the case of the $\{\text{Fe}(\text{pz})[\text{M}(\text{CN})_4]\} \cdot \text{H}_2\text{O}$ and $\{\text{Fe}(\text{azpy})[\text{M}(\text{CN})_4]\} \cdot \text{H}_2\text{O}$ ($\text{M} = \text{Pd}$ and Pt) series. Upon dehydration, the transition temperatures of the former increase up to 100 K and the hysteresis widens by up to 25 K,^[2a] whereas in the latter the transition temperatures decrease by 100 K and the hysteresis widens by 10 K.^[9] These data confirm the occurrence of stronger cooperativity in the bpac derivatives. All these results clearly demonstrate the strong effect of water molecules on the properties of this family of compounds and more generally the effect of solvent molecules on the spin-crossover phenomenon. Moreover, the higher T_c values obtained for the dehydrated form of the pyrazine and bpac homologues than with the azpy derivative could be explained by a more significant internal pressure of the three-dimensional network induced by the more important rigidity of the ligand, which also accounts for the stabilization of the LS state. Subsequently to the dehydration process, the evolution of the behavior of the nickel derivative is different from those of the platinum and palladium derivatives; indeed, sample **3d** shows a gradual and incomplete spin crossover centered at 220 K. The general significant differences obtained for the nickel complex (already reported for the azopyridine derivatives) seem to be related to structural modifications that originate in the smaller ionic radius in the case of Ni^{2+} . Figure 7 shows the comparison of the thermal dependence of the $\chi_M T$ product of hydrated (**1'**, **1'**, **4'**, and **4**) and dehydrated (**1''d**, **1'd**, **4'd**, and **4d**) forms of the platinum derivatives synthesized following the two different methods with increasing quantity of included bpac molecules (x). Clear evolution of the SCO behavior can be observed between the four complexes. Although the temperatures of the transition are similar ($T_c = 303, 302, 298, 297 \text{ K}$,

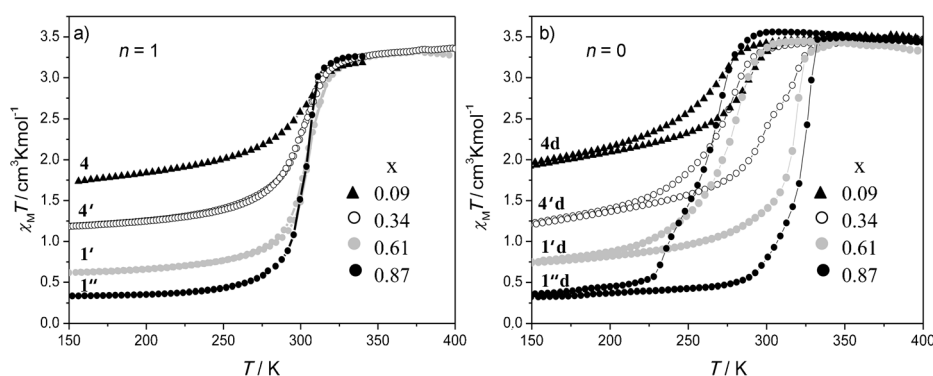


Figure 7. Magnetic properties, in the form of $\chi_M T$ versus T curves, of $\{\text{Fe}(\text{bpac})[\text{Pt}(\text{CN})_4]\}$ powders upon heating and cooling synthesized following method A (**1'** and **1''** ($n=1$), **1'd** and **1''d** ($n=0$)) and method B (**4** and **4'** ($n=1$), **4d** and **4'd** ($n=0$)) with increasing amount of included bpac molecules.

$T_c \downarrow = 262$ and $T_c \uparrow = 282$; for **1''**, **1'**, **4'**, and **4**, respectively. The cooperativity of the network is thus improved by both the absence of inserted water molecules and the presence of guest bpac molecules.

Mössbauer spectroscopy: Representative ^{57}Fe Mössbauer spectra of **1** and **4** (317 and 80 K) recorded in the cooling mode are shown in Figure 8 and values of the Mössbauer parameters obtained by least-

for **1''**, **1'**, **4'**, and **4**, respectively), increasingly gradual and incomplete spin transitions occur when passing from **1''** to **4**. These observations reveal a less cooperative behavior and the presence of an important residual HS iron(II) fraction as demonstrated by the high $\chi_M T$ product at 150 K of $1.75 \text{ cm}^3 \text{ K}$ for **4**. This effect is clearly correlated with the proportion of bpac molecules included within the pores. The important finding here is that the increase of the quantity of included bpac molecules in the network corresponds to the increase of the completeness of the spin transition. In other words, based on the features of the spin transition of compounds with different stoichiometry, the complete and cooperative spin transition seems to imply the presence of

approximately one included bpac molecule per iron atom, whereas a lower quantity leads to incomplete transitions. When the quantity of included molecules tends towards zero, the compound undergoes only a half spin transition. Even though structural determination of compound **4** was not possible, there is strong evidence from Raman and Mössbauer measurements (see below) that the strong rigidity of the network leads to a compressed structure that can only be accommodated by an asymmetrical coordination of the bridging bpac ligand, which leads to the occurrence of two distinct iron centers, with only one being spin-crossover active. For each compound, the dehydration process reveals hysteresis loops of 63, 42, 28, and 20 K while slightly decreasing the transition temperature with $T_c \downarrow = 262$ and $T_c \uparrow = 325$; $T_c \downarrow = 274$ and $T_c \uparrow = 316$; $T_c \downarrow = 272$ and $T_c \uparrow = 300$;

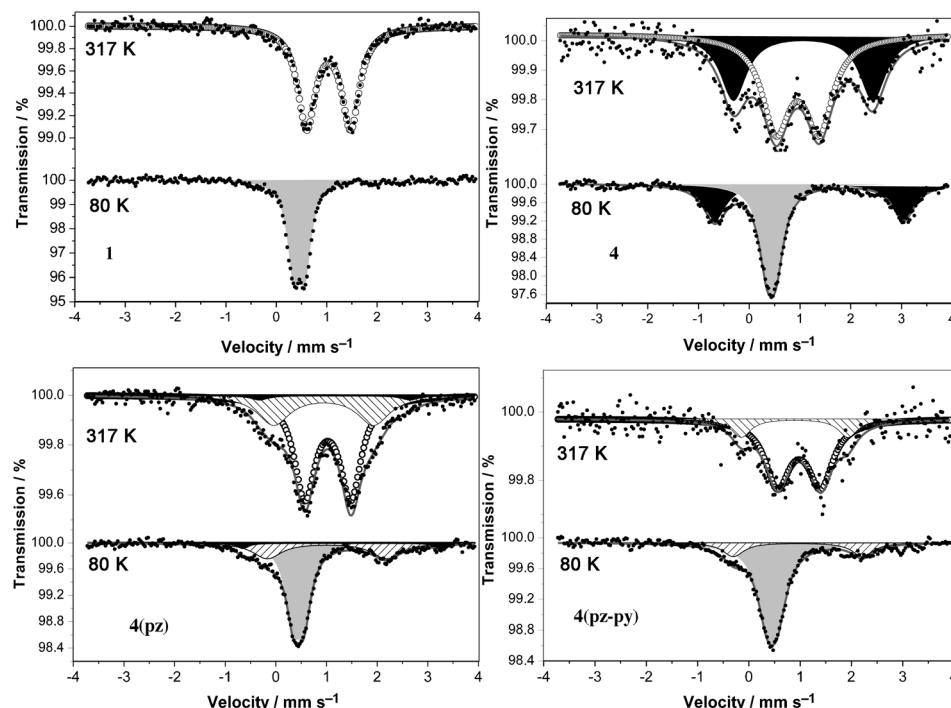


Figure 8. ^{57}Fe Mössbauer spectra of **1**, **4**, **4(pz)** and **4(pz-py)** in the high- and low-spin states.

squares fitting of the spectra are gathered in Table 1. At 317 K, the Mössbauer spectrum of **1** consists of a unique quadrupole-split doublet, with an isomer shift (δ) of $1.039(2) \text{ mm s}^{-1}$ and a quadrupole splitting (ΔE_Q) of $0.874(2) \text{ mm s}^{-1}$, in agreement with an iron(II) species in the HS state. The hyperfine parameters obtained from the least-squares fitting procedure of the spectra recorded at 80 K can be fitted with a doublet with $\delta = 0.4558(1) \text{ mm s}^{-1}$ and $\Delta E_Q = 0.2391(8) \text{ mm s}^{-1}$ in agreement with iron(II) in the LS state. The two spectra demonstrate the absence of residual LS and HS fractions at high and low temperature, respectively. Different features supporting the results of the magnetic measurements were obtained for sample **4** (method B). At 317 K, the Mössbauer spectrum is composed of two different doublets that can be attributed to iron(II) in the HS

Table 1. Representative least-squares-fitted ^{57}Fe Mössbauer data for **1**, **4**, **4(pz)**, and **4(pz-py)**.^[a]

Sample	<i>T</i> [K]	HS (site A)				HS (site B)				HS (site C)				LS				
		δ	ΔE_Q	$\Gamma/2$	%	δ	ΔE_Q	$\Gamma/2$	%	δ	ΔE_Q	$\Gamma/2$	%	δ	ΔE_Q	$\Gamma/2$	%	
1	317	1.039(1)	0.874(2)	0.147(4)	100													
	80									0.45(1)	0.239(8)	0.215(5)	100					
4	317	0.96(3)	0.85(4)	0.33(3)	59(1)	1.06(3)	2.75(6)	0.32(3)	41(1)									
	80					1.18(1)	3.72(3)	0.27(3)	43(2)	0.4378(6)	0.18*	0.192(1)	57(1)					
4(pz)	317	1.027(9)	0.90(2)	0.25*	67(3)	1.1(2)	2.97(4)	0.2*	2.3(2)	0.94(4)	2.0(1)	0.39(1)	30.7(9)					
	80					1.29(6)	3.9(1)	0.13(1)	3.9(3)	1.00(4)	2.35(8)	0.35(7)	31.3(6)	0.452(7)	0.20(2)	0.18(1)	64.8(3)	
4(pz-py)	317	0.99(3)	0.84(6)	0.29(5)	81(11)					0.89(9)	2.1(2)	0.23*	19(8)					
	80					0.96(3)	2.52(7)	0.25*	20(2)	0.453(7)	0.20(3)	0.23(2)	80(3)					

[a] Isomer shifts (δ in mm s^{-1}) refer to metallic iron at room temperature; ΔE_Q = quadrupole splitting [mm s^{-1}]; $\Gamma/2$ = half width of the lines at half height [mm s^{-1}]. Statistical standard deviations are given in parentheses; values with an asterisk were fixed during the fitting procedure.

state. The low $0.86(4) \text{ mm s}^{-1}$ value of ΔE_Q indicates that the local symmetry is lower than cubic and the ground orbital state is rather a doublet, which corresponds to an axial elongation of the octahedral environment around the iron center. Conversely, the large $2.75(6) \text{ mm s}^{-1}$ ΔE_Q value indicates a local symmetry lower than cubic, but with a rather well-isolated ground orbital singlet (in a well-isolated singlet case, ΔE_Q is in the $3\text{--}4 \text{ mm s}^{-1}$ range), which corresponds to an axial compression of the octahedral structure. When decreasing the temperature, at 80 K, the doublet with the smaller quadrupole splitting (similar to sample **1**), was transformed into the LS state, whereas the second doublet was not affected by the spin-state change. These results are in agreement with those of the magnetic studies and the X-ray crystal structure determination. In the case of **1** (equivalent composition to the single crystals of **5**), the large amount of included bpac molecules in the network involved in $\pi\text{--}\pi$ stacking interactions with the coordinated bpac molecules decreases the electron density of the bridging ligand and thus explains the elongation of almost all the axial Fe–N bonds, which represent the SCO-active Fe^{II} centers. By contrast, for sample **4**, only a small amount of guest bpac molecules are included within the network; a proportion of the iron centers in which the coordinated bpac is not involved in $\pi\text{--}\pi$ stacking interactions conserves an axial compression consistent with the inactive iron(II) centers revealed by magnetic and Mössbauer measurements. Moreover, the important ΔE_Q variation ($2.75(6)\text{--}3.72(3) \text{ mm s}^{-1}$) of the non-active HS doublet between 317 and 80 K is characteristic of a strongly distorted equatorial environment associated with a small energy gap between the d_{xy} orbital and the thermally accessible d_{xz} or d_{yz} orbitals.

Inclusion of guest molecules: All these results make evident the high sensitivity of the spin transition in this family of complexes to the quantity and the type of guest molecules, which has been specifically demonstrated by the effect of water and bpac molecules. Similar chemoresponsive effects have been observed in the corresponding nanoporous metal–organic framework $\{\text{Fe}(\text{pz})[\text{M}(\text{CN})_4]\}$ ($\text{M} = \text{Pt}, \text{Ni}, \text{Pd}$).^[5] Concerning the inclusion of water molecules, complementary thermogravimetric analysis has been performed to prove the reversible adsorption of water in **1** (Figure 9). The

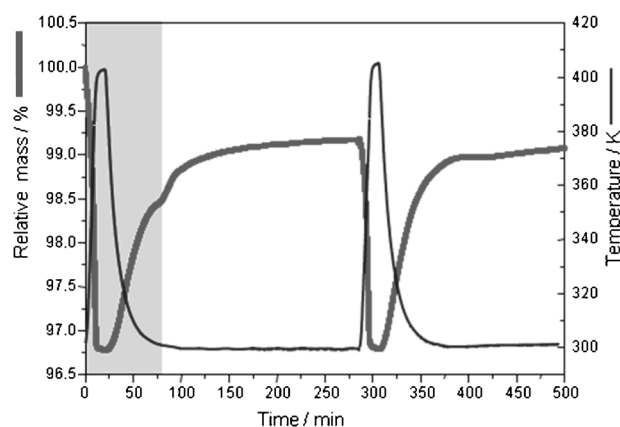


Figure 9. Representative thermogravimetric analysis revealing dehydration and rehydration kinetics for **1**.

sample has been heated at 10 K min^{-1} from room temperature until 400 K, which confirmed the loss of approximately one molecule of water per iron atom. Then, the system was cooled under a stream of dry air (containing only traces of water), which led to the partial recovery of water molecules (gray area in the diagram). Following the small plateau, the sample was exposed to atmospheric air (white area) showing additional adsorption of water. A second cycle $293 \rightarrow 400 \rightarrow 293 \text{ K}$ has been fully realized under atmospheric air and readsorption of the majority of water molecules occurs in approximately one hour; complete recovery of the initial composition takes 24 h.

To extend this work, we have investigated the susceptibility of the framework to accept inclusions other than water or bpac molecules and we have studied the synergy between host–guest chemistry and spin-crossover behavior. Two strategies have been developed, either by preparing crystals by slow liquid–liquid diffusion in the presence of aromatic molecules that compete with the bpac molecules^[3a] or by putting powder samples synthesized following method B in contact with pyrazine or pyridine vapors. Following the latter strategy, further vapor adsorption experiments were performed with powder samples $\{\text{Fe}(\text{bpac})[\text{Pt}(\text{CN})_4]\}$ prepared by method B (samples **4** and **4'**). Sample **4** was treated overnight by pyrazine vapor and the resulting **4(pz)** sample was

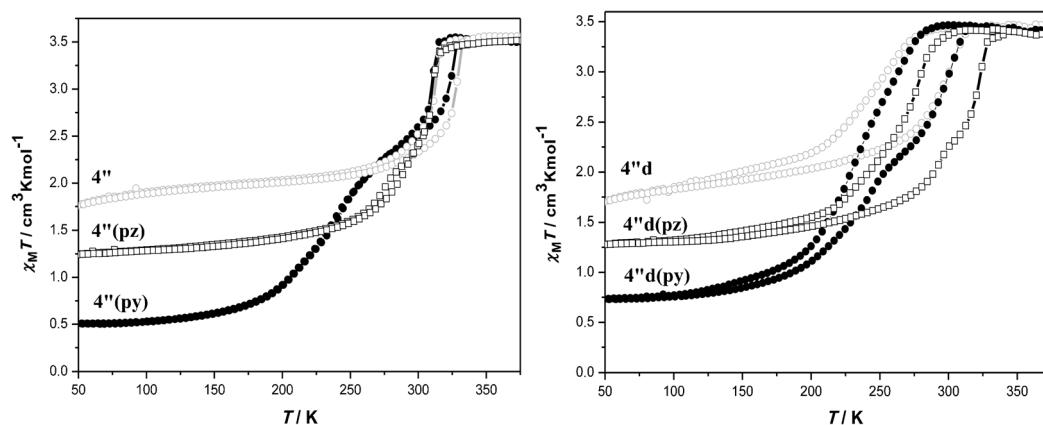


Figure 10. Temperature dependence of $\chi_M T$ for $4''$, $4''(\text{py})$, and $4''(\text{pz})$ and the dehydrated forms $4''\text{d}$, $4''\text{d}(\text{py})$, and $4''\text{d}(\text{pz})$.

studied by Mössbauer spectroscopy. Figure 8 shows the Mössbauer spectrum of $4(\text{pz})$ acquired at 317 and 80 K and values of the Mössbauer parameters obtained by least-squares fitting of the spectra are gathered in Table 1 and compared with those of samples **1** and **4**. At 317 K the spectrum can be satisfactorily fitted by considering three quadrupole-split doublets with isomer shift and quadrupole-splitting values attributable to iron(II) in the high-spin state. In comparison with sample **4**, the pyrazine vapor that enters the network modifies the environment of the majority of the iron(II) centers, so that the intensity of the doublet with the large ΔE_Q (site B, doublet in black) decreases drastically. Conversely, the proportion of the doublet with the small ΔE_Q (site A) increases slightly (from 59 to 67%) and a new doublet with intermediate $\Delta E_Q = 2.0(1) \text{ mms}^{-1}$ (site C) appears. At low temperature, a LS iron(II) doublet appears: its parameters are $\delta = 0.452(7) \text{ mms}^{-1}$ and $\Delta E_Q = 0.21(2) \text{ mms}^{-1}$ and similarly to sample **4**, only the HS doublet with the smallest quadrupole splitting is affected by the spin transition. In fact, in $4(\text{pz})$, only a small amount of pyrazine entered the structure, as demonstrated by the thermogravimetric analysis coupled with mass spectroscopy of the analogous compound $4''(\text{pz})$ (see below). As a consequence only a small proportion of the inactive sites B were transformed into active sites A (8%). This probably occurs because of π - π stacking interactions between the aromatic rings of pyrazine molecules and those of the two bpac ligand moieties around the considered iron atom. Moreover, even if a small proportion (about 3%) is not affected by the pyrazine inclusion, the remaining population is transformed to site C (about 31%), which corresponds to inactive iron atoms with certainly only one bpac ligand involved in π - π stacking interactions. It is interesting to note the intermediate value of ΔE_Q for site C versus those of sites A and B, and its moderate thermal variation ($2.0(1)$ – $2.35(8) \text{ mms}^{-1}$) compared to site B. This corresponds to a rather well-isolated ground orbital singlet (weak mean axial compression) with a weakly distorted equatorial environment associated with a large energy gap between the d_{xy} orbital and the thermally accessible d_{xz} or d_{yz} orbitals. Further Mössbauer inves-

tigation was performed following the exposure of sample $4(\text{pz})$ to pyridine vapor, thereby leading to sample $4(\text{pz-py})$. The Mössbauer spectrum of $4(\text{pz-py})$ at 317 K (Figure 8) reveals, in comparison with sample $4(\text{pz})$, the disappearance of site B and the decrease of site C with a concomitant increase of the proportion of active site A. In this case also, at 80 K, the whole fraction of site A (about 80%) was converted into iron(II) LS centers while the fraction of site B remained in the HS state. Thermogravimetric analysis coupled with mass spectroscopy (TGA-MS) measurement at m/z 78 makes evident that 0.75 pyridine molecules per iron atom were present in compound $4''(\text{py})$ and the same measurements at m/z 80 reveals that 0.45 pyrazine molecules per iron atom was present in compound $4''(\text{pz})$ (Figure S5 in the Supporting Information). Figure 10 shows the magnetic behavior of compound $4''$ before and after the adsorption of pyridine ($4''(\text{py})$) or pyrazine ($4''(\text{pz})$) vapors in their hydrated and dehydrated forms. In agreement with the magnetic result of sample **4**, sample $4''$ exhibits a cooperative and incomplete spin transition centered at 318 K (with a hysteresis of 14 K). Significant change can be observed in sample $4''(\text{pz})$: the magnetic curve reveals a spin transition in two steps ($T_{c1} = 282 \text{ K}$ and $T_{c2} = 310 \text{ K}$) and the $\chi_M T$ value of $1.25 \text{ cm}^3 \text{ K mol}^{-1}$ at 80 K indicates a lower residual HS fraction. The same effect but with amplification of the phenomenon has been measured for $4''(\text{py})$. In this case, the second step is more complete with a transition temperature T_{c2} shifted to 233 K. These results clearly demonstrate that the origin of the two-step transition in these compounds is related to the presence of two different iron centers with the value of T_{c2} depending on the vicinity of the iron centers with either bpac or pyridine guest molecules. The more complete nature of the spin transition for $4''(\text{py})$ versus $4''(\text{pz})$ is related to the larger fraction of included pyridine molecule than that of pyrazine molecule. As already mentioned, the dehydration process tends to increase the size of the hysteresis loop and decreases the transition temperature without modifying the completeness of the transitions.

Conclusion

We have investigated a series of 3D Hofmann-like clathrate metal–organic frameworks exhibiting spin crossover at room temperature with significant hysteresis loops (up to 68 K). The main finding of this paper is that the physical and spectroscopic characterization of $\{\text{Fe}(\text{bpac})[\text{M}(\text{CN})_4]\cdot\text{H}_2\text{O}\cdot x(\text{bpac})$ ($\text{M} = \text{Pt}, \text{Pd}, \text{and Ni}$) allowed us to observe how structural characteristics, Raman and Mössbauer spectral features, and the spin transition vary with the sample stoichiometry. In samples with a low proportion of included bpac molecules, the occurrence of different iron centers leads to incomplete and less-cooperative spin transitions. Conversely, when a large proportion of bpac molecules are included, the π – π stacking interaction between the bridging and included bpac molecules tends to homogenize the network and complete and cooperative spin transitions are observed. Another new feature reported here is that the room temperature ^{57}Fe Mössbauer spectra give a direct measure of the amount of spin-transition-active material present in the sample. The part of the material that is spin-transition active shows a doublet with a small quadrupole splitting ($\approx 0.9 \text{ mm s}^{-1}$) for HS Fe^{II} . Vapor-adsorption experiments on powdered samples of these 3D compounds revealed the susceptibility of the framework to accept guests other than water or bpac molecules. The physical studies of the modified networks showed the synergy between host–guest chemistry and spin-crossover behavior. Indeed, the clathration of various aromatic molecules revealed specific modification of the transition temperature. These preliminary results confirm the high sensitivity of these highly porous compounds towards gas and vapors, already demonstrated for the pyrazine derivative⁵¹ and open new opportunities for the elaboration of gas-sensor technologies.

Experimental Section

Materials: $\text{K}_2[\text{Pd}(\text{CN})_4]\cdot n\text{H}_2\text{O}$, $\text{K}_2[\text{Pt}(\text{CN})_4]\cdot 3\text{H}_2\text{O}$, $\text{K}_2[\text{Ni}(\text{CN})_4]\cdot n\text{H}_2\text{O}$, and $\text{Fe}(\text{BF}_4)_2\cdot 6\text{H}_2\text{O}$ salts and solvents were purchased from commercial sources and used as received. The synthesis of the bis(4-pyridyl)acetylene (bpac) ligand was carried out according to Ref. [3a].

Synthesis of $[\text{Fe}(\text{bpac})\text{M}(\text{CN})_4]\cdot\text{H}_2\text{O}\cdot x(\text{bpac})$ ($\text{M} = \text{Pt}$ (1), Pd (2), and Ni (3))—method A: The syntheses were performed under an argon atmosphere. A methanolic solution of bpac (0.222 mmol, 20 mL) was added to a solution of $\text{Fe}(\text{BF}_4)_2\cdot 6\text{H}_2\text{O}$ in methanol/water (1:1) (0.222 mmol, 20 mL). $\text{K}_2[\text{M}(\text{CN})_4]$ (0.222 mmol) dissolved in water (20 mL) was added dropwise to the resulting yellow solution leading instantaneously to the formation of yellow-orange precipitates. The precipitates were filtered off and washed with methanol and H_2O and subsequently dried under vacuum. Yields: 51, 59, 47, 50, and 64% for **1**, **1'**, **2** and **3**, respectively. Elemental analyses calcd (%) for $[\text{Fe}(\text{bpac})[\text{Pt}(\text{CN})_4]]\cdot\text{H}_2\text{O}\cdot 0.71(\text{bpac})$ (**1**): C 43.22, N 15.26, H 2.30, Pt 28.66, Fe 8.20; found: C 43.22, N 14.71, H 2.03, Pt 27.95, Fe 8.11, Pt/Fe = 0.986; calcd (%) for $[\text{Fe}(\text{bpac})[\text{Pt}(\text{CN})_4]]\cdot\text{H}_2\text{O}\cdot 0.61(\text{bpac})$ (**1'**): C 42.28, N 15.25, H 2.25, Pt 29.39, Fe 8.41; found: C 42.28, N 14.54, H 1.73, Pt 28.79, Fe 8.45, Pt/Fe = 0.976; calcd (%) for $[\text{Fe}(\text{bpac})[\text{Pt}(\text{CN})_4]]\cdot\text{H}_2\text{O}\cdot 0.87(\text{bpac})$ (**1''**): C 44.72, N 15.27, H 2.39, Pt 27.49, Fe 7.87; found: C 44.72, N 15.32, H 2.09, Pt 27.92, Fe 7.89, Pt/Fe = 1.013; calcd (%) for $[\text{Fe}(\text{bpac})[\text{Pd}(\text{CN})_4]]\cdot\text{H}_2\text{O}\cdot 0.78(\text{bpac})$ (**2**): C 50.45, N 17.51, H 2.67; found: C 50.43, N 16.83, H 2.16; calcd (%)

for $[\text{Fe}(\text{bpac})[\text{Ni}(\text{CN})_4]]\cdot\text{H}_2\text{O}\cdot 0.40(\text{bpac})$ (**3**): C 51.11, N 19.48, H 2.71; found: C 51.10, N 18.10, H 2.26.

Synthesis of $[\text{Fe}(\text{bpac})\text{Pt}(\text{CN})_4]\cdot\text{H}_2\text{O}\cdot x(\text{bpac})$ (4**)—method B:** The synthesis was performed under an argon atmosphere. A solution of $\text{Fe}(\text{BF}_4)_2\cdot 6\text{H}_2\text{O}$ (0.222 mmol) and bpac (0.222 mmol) in methanol/water (1:1, 20 mL) was added dropwise to an aqueous solution of $\text{K}_2[\text{Pt}(\text{CN})_4]$ (0.222 mmol) leading to the formation of yellow-orange precipitates. The precipitates were filtered off and washed with methanol and H_2O and subsequently dried under vacuum. Yields: 75 and 66% for **4** and **4'**, respectively. Elemental analysis calcd (%) for $[\text{Fe}(\text{bpac})[\text{Pt}(\text{CN})_4]]\cdot\text{H}_2\text{O}\cdot 0.09(\text{bpac})$ (**4**): C 36.02, N 15.20, H 1.88, Pt 34.27, Fe 9.81; found: C 36.12, N 14.52, H 1.54, Pt 33.38, Fe 9.62, Pt/Fe = 0.993; calcd (%) for $[\text{Fe}(\text{bpac})[\text{Pt}(\text{CN})_4]]\cdot\text{H}_2\text{O}\cdot 0.34(\text{bpac})$ (**4'**): C 39.25, N 15.23, H 2.07, Pt 31.75, Fe 9.09; found: C 39.27, N 14.59, H 1.77, Pt 34.06, Fe 9.94, Pt/Fe = 0.980.

Inclusion experiments: Vapor-adsorption experiments were carried out on freshly prepared powder samples **4** and **4''** (obtained using method B). The powder was placed into a small, open vessel. This vessel was placed in a larger sealed vessel containing pyrazine ($\approx 3 \text{ mg}$ in the case of **4** and **4''**) or pyridine (approximately 3 mL in the case of sample **4''**). This setup was gently heated and maintained at 35°C for one night, causing the vaporization and sublimation of pyridine and pyrazine, respectively. After the adsorption experiments, samples **4(pz)**, **4(pz-py)**, **4''(pz)**, and **4''(py)** were recovered and their properties were analyzed by Mössbauer or magnetic measurements.

Microanalyses: Analysis for C, H, and N were performed after combustion at 850°C using IR detection and gravimetry by means of a Perkin–Elmer 2400 series II device. Analysis for Fe, Pt, and B were performed by means of a Thermo Scientific iCAP 6000 Series ICP emission spectrometer.

Thermal analysis: Differential thermal analysis and thermogravimetric (DTA–TG) data were acquired simultaneously using a Perkin–Elmer Diamond thermal analyzer. Coupled mass spectrometry analyses of elements were realized with a Pfeiffer Vacuum Omnistar quadrupole mass spectrometer.

X-ray powder diffraction: The powder X-ray diffraction patterns were collected on a XPert Pro (Theta-Theta mode) Analytical diffractometer with $\lambda(\text{Cu}_{\text{K}\alpha 1}, \text{Cu}_{\text{K}\alpha 2}) = 1.54059, 1.54439 \text{ \AA}$. Variable-temperature measurements were performed on an Antoon Paar TTK 450 Chamber, from room temperature to 400 K. The extraction of peak positions for indexing was performed with the fitting program, available in the PC software package Highscore+ supplied by Panalytical. Pattern indexing was carried out by means of the program DICVOL implemented in the Highscore+ package. The cell refinement was also performed using Highscore+.

Magnetic studies: The magnetic properties were measured at various cooling and heating rates under a field of 1 T using a Quantum Design MPMS superconducting quantum interference device magnetometer. The experimental data were corrected for the diamagnetic contribution.

DSC analysis: DSC analysis was carried out on a Netzsch DSC 204 instrument under helium purging gas ($20 \text{ cm}^3 \text{ min}^{-1}$) at a heating/cooling rate of 10 K min^{-1} . Temperature and enthalpy were calibrated using the melting transition of standard materials (Hg, In, Sn). The uncertainty in the transition enthalpy (ΔH_{HL}) and entropy (ΔS_{HL}) is estimated to be approximately 10% due to the subtraction of the unknown baseline.

Raman spectroscopy: Raman spectra were collected between 300 and 80 K using a LabRAM-HR (Jobin–Yvon) Raman micro-spectrometer and a Linkam THMS-600 cryostage. The 632.8 nm line of a He–Ne laser was used as the excitation source and a spectral resolution of approximately 3 cm^{-1} was obtained.

Mössbauer spectroscopy: ^{57}Fe Mössbauer spectra have been recorded using a conventional constant-acceleration-type spectrometer equipped with a 50 mCi ^{57}Co source and a flow-type, liquid-helium cryostat. Spectra of the powder samples (ca. 30 mg) were recorded between 5 and 300 K. Least-squares fittings of the Mössbauer spectra have been carried out with the assumption of Lorentzian line shapes using the Recoil software package.

Acknowledgements

This work was supported by the CHEMOSWITCH project (ANR 2010-BLAN-1018 01), the BISTABLE project (University Paul Sabatier PRES), the Spanish Ministerio de Ciencia e Innovación (MICINN), and FEDER funds (CTQ2010-18414) and the Generalitat Valenciana (GVA-COMP2010-139). N.A.O.V. thanks the Instituto de Ciencia y Tecnología del DF (iCyTDF) in Mexico for a postdoctoral fellowship and C.B.M. thanks the French Embassy in Spain and the Caixa for a doctoral fellowship.

- [1] a) D. Zacher, R. Schmid, C. Wöll, R. A. Fischer, *Angew. Chem.* **2011**, *123*, 184–208; *Angew. Chem. Int. Ed.* **2011**, *50*, 176–199; b) C. Janiak, J. K. Vieth, *New J. Chem.* **2010**, *34*, 2366–2388; c) Special issue: Metal–Organic Frameworks, J. Long, O. Yaghi, *Chem. Soc. Rev.* **2009**, *38*, Issue 5; d) D. MasPOCH, D. Ruiz-Molina, J. Veciana, *Chem. Soc. Rev.* **2007**, *36*, 770–818.
- [2] a) V. Niel, J. M. Martínez-Agudo, M. C. Muñoz, A. B. Gaspar, J. A. Real, *Inorg. Chem.* **2001**, *40*, 3838–3839; b) G. J. Halder, C. J. Kepert, B. Moubaraki, K. S. Murray, J. D. Cashion, *Science* **2002**, *298*, 1762–1765; c) A. Bousseksou, G. Molnár, L. Salmon, W. Nicolazzi, *Chem. Soc. Rev.* **2011**, *40*, 3313–3335; d) M. C. Muñoz, J. A. Real, *Coord. Chem. Rev.* **2011**, 2068–2095; e) J. A. Real, E. Andrés, M. C. Muñoz, M. Julve, T. Granier, A. Bousseksou, F. Varret, *Science*, **1995**, *268*, 265–267.
- [3] a) C. Bartual-Murgui, N. Ortega-Villar, H. J. Shepherd, M. C. Muñoz, L. Salmon, G. Molnár, A. Bousseksou, J. A. Real, *J. Mater. Chem.* **2011**, *21*, 7217–7222; b) T. Tayagaki, A. Galet, G. Molnár, M. C. Muñoz, A. Zwick, K. Tanaka, J. A. Real, A. Bousseksou, *J. Phys. Chem. B* **2005**, *109*, 14859–14867.
- [4] a) S. Bonhommeau, G. Molnár, A. Galet, A. Zwick, J. A. Real, J. J. McGarvey, A. Bousseksou, *Angew. Chem.* **2005**, *117*, 4137–4141; *Angew. Chem. Int. Ed.* **2005**, *44*, 4069–4072; b) S. Cobo, D. Ostrovskii, S. Bonhommeau, L. Vendier, G. Molnár, L. Salmon, K. Tanaka, A. Bousseksou, *J. Am. Chem. Soc.* **2008**, *130*, 9019–9024.
- [5] a) M. Ohba, K. Yoneda, G. Agustí, M. C. Muñoz, A. B. Gaspar, J. A. Real, M. Yamasaki, H. Ando, Y. Nakao, S. Sakaki, S. Kitagawa, *Angew. Chem.* **2009**, *121*, 4861–4865; *Angew. Chem. Int. Ed.* **2009**, *48*, 4767–4771; b) G. Agustí, R. Ohtani, K. Yoneda, A. B. Gaspar, M. Ohba, J. F. Sánchez-Royo, M. C. Muñoz, S. Kitagawa, J. A. Real, *Angew. Chem.* **2009**, *121*, 9106–9109; *Angew. Chem. Int. Ed.* **2009**, *48*, 8944–8947; c) P. D. Southon, L. Liu, E. A. Fellows, D. J. Price, G. J. Halder, K. W. Chapman, B. Moubaraki, K. S. Murray, J. F. Létard, C. J. Kepert, *J. Am. Chem. Soc.* **2009**, *131*, 10998–11009.
- [6] I. Boldog, A. B. Gaspar, V. Martínez, P. Pardo-Ibáñez, V. Ksenofontov, A. Bhattacharjee, P. Gütllich, J. A. Real, *Angew. Chem.* **2008**, *120*, 6533–6537; *Angew. Chem. Int. Ed.* **2008**, *47*, 6433–6437.
- [7] a) F. Volatron, L. Catala, E. Rivière, A. Gloter, O. Stephan, T. Mallah, *Inorg. Chem.* **2008**, *47*, 6584–6586; b) J. Larionova, L. Salmon, Y. Guari, A. Tokarev, K. Molvinger, G. Molnár, A. Bousseksou, *Angew. Chem.* **2008**, *120*, 8360–8364; *Angew. Chem. Int. Ed.* **2008**, *47*, 8236–8240.
- [8] a) S. Cobo, G. Molnár, J. A. Real, A. Bousseksou, *Angew. Chem.* **2006**, *118*, 5918–5921; *Angew. Chem. Int. Ed.* **2006**, *45*, 5786–5789; b) G. Molnár, S. Cobo, J. A. Real, F. Carcenac, E. Daran, C. Vieu, A. Bousseksou, *Adv. Mater.* **2007**, *19*, 2163–2167; c) C. Bartual-Murgui, L. Salmon, A. Akou, C. Thibault, G. Molnár, T. Mahfoud, Z. Sekkat, J. A. Real, A. Bousseksou, *New J. Chem.* **2011**, *35*, 2089–2094.
- [9] G. Agustí, S. Cobo, A. B. Gaspar, G. Molnár, N. O. Moussa, P. Á. Szilágyi, V. Pálfi, C. Vieu, M. C. Muñoz, J. A. Real, A. Bousseksou, *Chem. Mater.* **2008**, *20*, 6721–6732.
- [10] H. J. Shepherd, C. Bartual-Murgui, G. Molnár, J. A. Real, M. C. Muñoz, L. Salmon, A. Bousseksou, *New J. Chem.* **2011**, *35*, 1205–1210.
- [11] a) K. Kondo, N. Ohnishi, K. Takemoto, H. Yoshida, K. Yoshida, *J. Org. Chem.* **1992**, *57*, 1622–1625; b) H. L. Anderson, C. J. Walter, A. Vidal-Ferran, R. A. Hay, P. A. Lowden, J. K. M. Sanders, *J. Chem. Soc. Perkin Trans. 1 (1972–1999)* **1995**, 2275–2280; c) N. R. Champness, A. N. Khlobystov, N. Andrei, A. G. Majuga, M. Schroeder, N. V. Zyk, *Tetrahedron Lett.* **1999**, *40*, 5413–5416; d) B. J. Coe, J. L. Harries, J. A. Harris, B. S. Brunschwig, S. J. Coles, M. E. Light, M. B. Hursthouse, *Dalton Trans.* **2004**, 2935–2942.
- [12] N. Inoue, O. Sugimoto, K. Tanji, *Heterocycles* **2007**, *72*, 665–671.
- [13] a) J. S. O. Evans, *J. Chem. Soc. Dalton Trans.* **1999**, 3317–3026; b) T. Pretsche, K. W. Chapman, G. J. Halder, C. J. Kepert, *Chem. Commun.* **2006**, 1857–1859.
- [14] P. Guionneau, M. Marchivie, G. Bravic, J.-F. Létard, D. Chasseau, *Top. Curr. Chem.* **2004**, *234*, 97–128.

Received: July 29, 2011

Published online: December 6, 2011